

Supplemental information

**Targeting allostery in the Dynein motor
domain with small molecule inhibitors**

Cristina C. Santarossa, Keith J. Mickolajczyk, Jonathan B. Steinman, Linas Urnavicius, Nan Chen, Yasuhiro Hirata, Yoshiyuki Fukase, Nicolas Coudray, Damian C. Ekiert, Gira Bhabha, and Tarun M. Kapoor

Table S1 Data collection and refinement statistics (molecular replacement),
Related to Figure 3

Sc-Dyn-lysoMut (PDB: 7MI1)	
Data collection	
Space group	<i>P2₁2₁2</i>
Cell dimensions	
<i>a</i> , <i>b</i> , <i>c</i> (Å)	135.06, 157.92, 179.31
α , β , γ (°)	90.00 90.00 90.00
Resolution (Å)	47.66-4.50 (4.77-4.50)
<i>R</i> _{meas}	28.6 (168.7)
<i>I</i> / σ	5.99 (1.13)
Completeness (%)	99.5 (98.3)
Redundancy	6.8 (6.5)
CC1/2	99.5 (48.4)
Refinement	
Resolution (Å)	50-4.5
No. reflections	23226
<i>R</i> _{work} / <i>R</i> _{free}	0.276/0.320
No. atoms	
Protein	42311
Ligand/ion	N/A
Water	N/A
<i>B</i> -factors	
Protein	207
Ligand/ion	N/A
Water	N/A
R.m.s. deviations	
Bond lengths (Å)	0.003
Bond angles (°)	0.052
Clashscore	6

Values are for a single crystal.

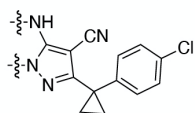
*Highest-resolution shell is shown in parentheses.

Table S2 Cryo-EM data collection and refinement statistics, Related to Figure 4

Data Collection	Dataset 1	Dataset 2	Dataset 3
Microscope	Titan Krios	Titan Krios	Titan Krios
Camera	K2 Summit	K2 Summit	K2 Summit
Voltage (kV)	300	300	300
Frames	50	50	50
Exposure time (s)	10	10	10
Total dose ($\bar{e}/\text{\AA}^2$)	71	52	44
Defocus range (μm)	-1.5 to -3	-0.9 to -1.7	-1 to -1.5
Super resolution pixel size (\AA)	0.6675	0.6675	0.518
No. of micrographs	1696	4518	4893

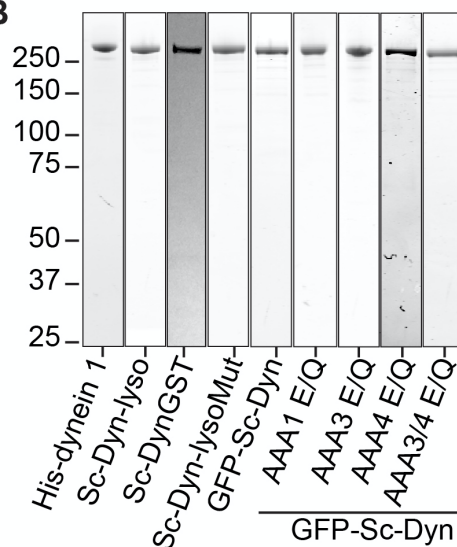
	Map 1 (Composite model)	Map 2 (AAA6s/AA A1/AAA2L)	Map 3 (AAA6s/AA A1/AAA2L)	Map 4 (Model 4)	Map 5 (Model 5)
Model composition					
EMD ID	23841	23844	23846	23838	23842
PDB ID	7MI6	--	--	7MI3	7MI8
Number of particles	136180	40854	7278	131702	128004
Non-hydrogen atoms	19653			9682	7034
Protein residues	2419			1192	868
Ligands (ATP/Compound 20)	1/2			1/2	0/0
Resolution (\AA , FSC=0.143)	~3.9	~4.7	~7.9	~3.5	~3.7
Map sharpening B-factors (\AA^2)	-100	-100	-50	-50	-100
Sphericity from 3D FSC	0.78	0.96	0.97	0.86	0.81
Mean B-factor (\AA^2)	117.19			140.91	40.33
rmsd (bonds)	0.012			0.010	0.006
rmsd (angles)	1.487			1.465	0.962
MolProbity score	1.83			1.94	1.99
Clashscore, all atoms	6.41			5.12	5.27
Rotamer outliers (%)	1.32			1.94	0.38
Ramachandran plot (%):					
Favored	94.32			92.85	97.45
Outliers	0.41			0.34	0.12
Map CC (mask)	0.76			0.86	0.76
Map CC (box)	0.83			0.85	0.81
Map CC (peaks)	0.69			0.76	0.72
Map CC (volume)	0.74			0.85	0.75
Map CC for ligands	0.85			0.88	--

A Structure-activity relationship for compounds with aminopyrazole core

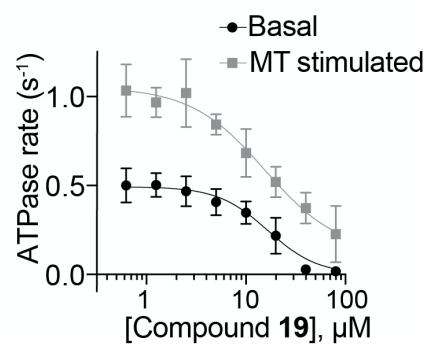


Compound	Substituents	Percent Residual ATPase activity (range)
3		115 (104-125)
4		115 (91-140)
5		104 (90-118)
6		100 (97-102)
7		99 (78-120)
8		97 (97-97)
9		92 (88-95)
10		89 (69-109)
11		87 (84-90)
12		80 (77-82)
13		79 (68-89)
14		76 (71-81)
15		75 (71-78)
16		70 (65-74)
17		51 (48-53)
18		49 (45-52)
19		32 (29-34)
20		32 (23-40)

B



C



D

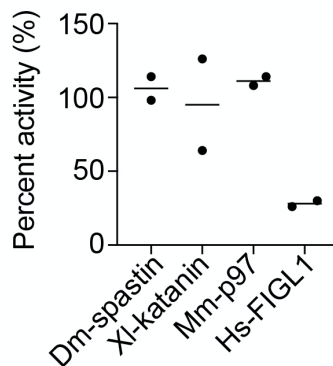


Figure S1. Structure-activity relationship studies of dynapyrazole derivatives, Related to Figure 1. (A) Basal ATPase activity of Hs-dynein 1 in the presence of dynapyrazole derivatives (20 μ M). Chemical structure of each dynapyrazole derivative is shown. (B) SDS-PAGE analysis of purified dynein constructs (Coomassie blue). Sample lanes are from different gels, as indicated by the border. (C) ATPase activity of Hs-dynein 1 in the presence of compound **19** with or without the addition of microtubules (2.5 μ M). Data are mean \pm SD of n=3 and were fit to a sigmoidal dose-response curve. (D) Percent steady-state ATPase activity of four AAA proteins in the presence of compound **19** (20 μ M). Lines represent mean (n=2). Mean for each construct is as follows: 106% (Dm-spastin), 95% (Xl-katanin), 111% (Mm-97), 28% (Hs-FIGL).

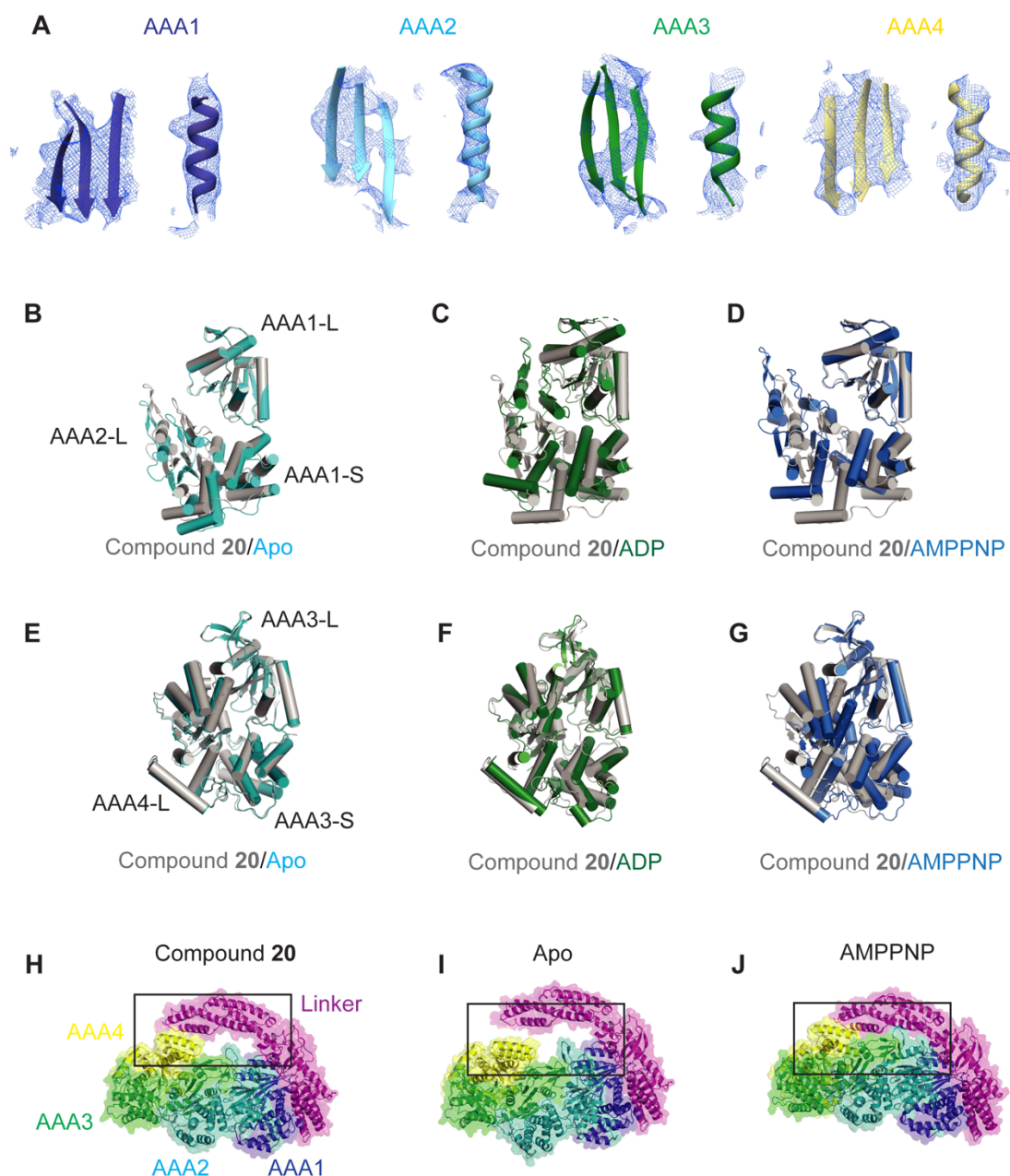


Figure S2. X-ray model of Sc-Dyn-lysoMut in the presence of compound 20, Related to Figure 3. (A) Electron densities (blue mesh, 1.0 σ contour) of β -strands and α -helices in the AAA1, AAA2, AAA3, and AAA4 sites. Color coding of domains is the same as in Figure 3A. (B-D) Comparison of the AAA1 domain between the X-ray model (gray) and the *S. cerevisiae* apo (cyan) (B), human ADP (PDB: 5NUG, green) (C), or *S. cerevisiae* AMPPNP (PDB: 4W8F, blue) (D) model. Models are aligned on the AAA1-L subdomain.

(E-G) Comparison of the AAA3 domain between the X-ray model (gray) and the *S. cerevisiae* apo (cyan) (E), human ADP (PDB: 5NUG, green) (F), or Sc-Dyn-lysoMut AMPPNP (PDB: 4W8F, blue) (G) model. Models are aligned on the AAA3-L subdomain.

(H-J) Comparison of one side of the AAA ring in the X-ray model (H), apo-model (I), and the AMPPNP-model (J) (PDB: 4W8F). The box highlights the gap between the linker and the AAA1/AAA2/AAA3/AAA4 domains. Color coding of domains is the same as in Figure 3A; models are aligned on the AAA1-L subdomain.

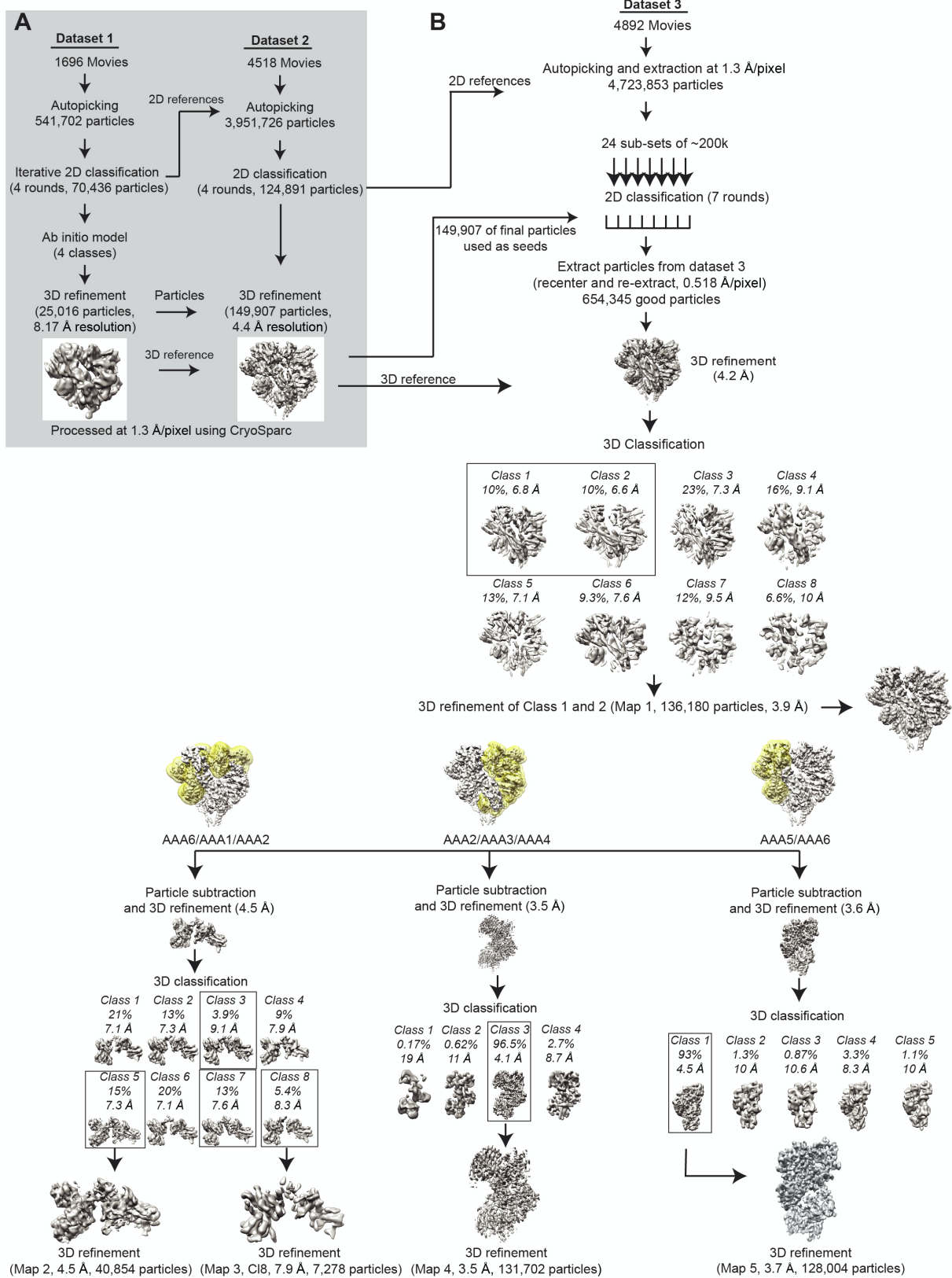


Figure S3. Processing of the Cryo-EM data for Sc-Dyn-lysoMut in the presence of compound 20, Related to Figure 4. (A) The workflow used to process datasets 1 and 2 in CryoSparc. (B) The workflow used to process dataset 3 in RELION 3.0.

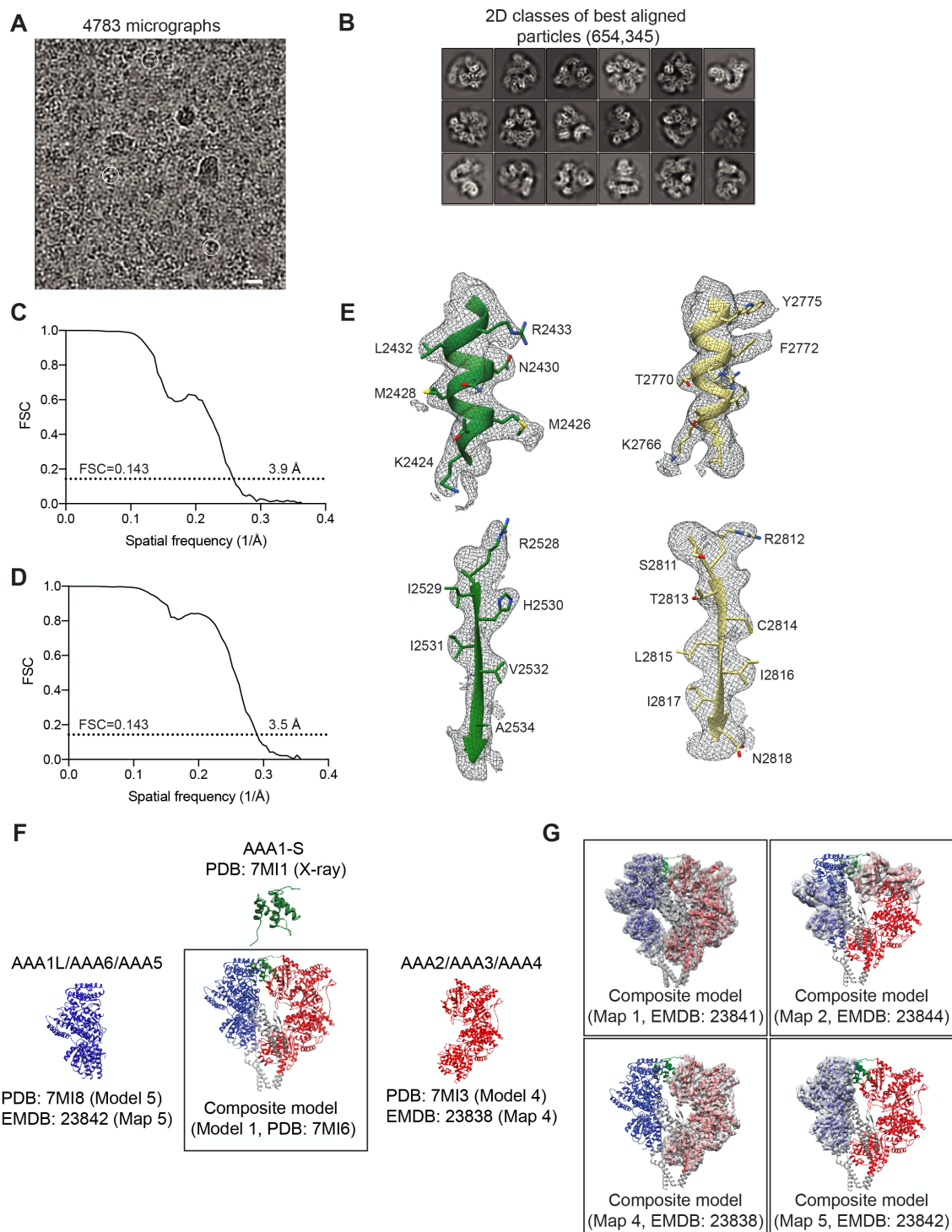


Figure S4. Cryo-EM analysis of Sc-Dyn-lysoMut in the presence of compound 20, Related to Figure 4. (A) Representative micrograph from dataset 3 (total: 4893 micrographs). Examples of particles picked are circled (white). White scale bar represents

20 nm. (B) 2D classes of best aligned particles (654,345). (C) Gold-standard Fourier Shell Correlation (FSC) curve calculated for Map 1 (See Figure S3B). The resolution was estimated at ~ 3.9 Å (FSC=0.143). (D) Gold-standard Fourier Shell Correlation (FSC) curve calculated for Map 4 (See Figure S3B). The resolution was estimated at ~ 3.5 Å (FSC=0.143). (E) EM densities (Map 4, gray mesh) of β -strands and α -helices in the AAA3 (green) and AAA4 (yellow) domains. Amino acid residues are indicated and the color coding of domains is the same as in Figure 3A. (F) Individual components of the composite model (Model 1) (See STAR methods). AAA2/AAA3/AAA4 (Model 4, red) were built into Map 4. AAA1L/AAA6/AAA5 and residues 1524-1760 of the linker (Model 5, blue) were built into Map 5. AAA1-S (green) as well as parts of the linker (residues 1365-1524) and stalk/buttruss (gray) were built based on the X-ray map. (G) Composite model fit into Map 1, Map 2, Map 4, or Map 5.

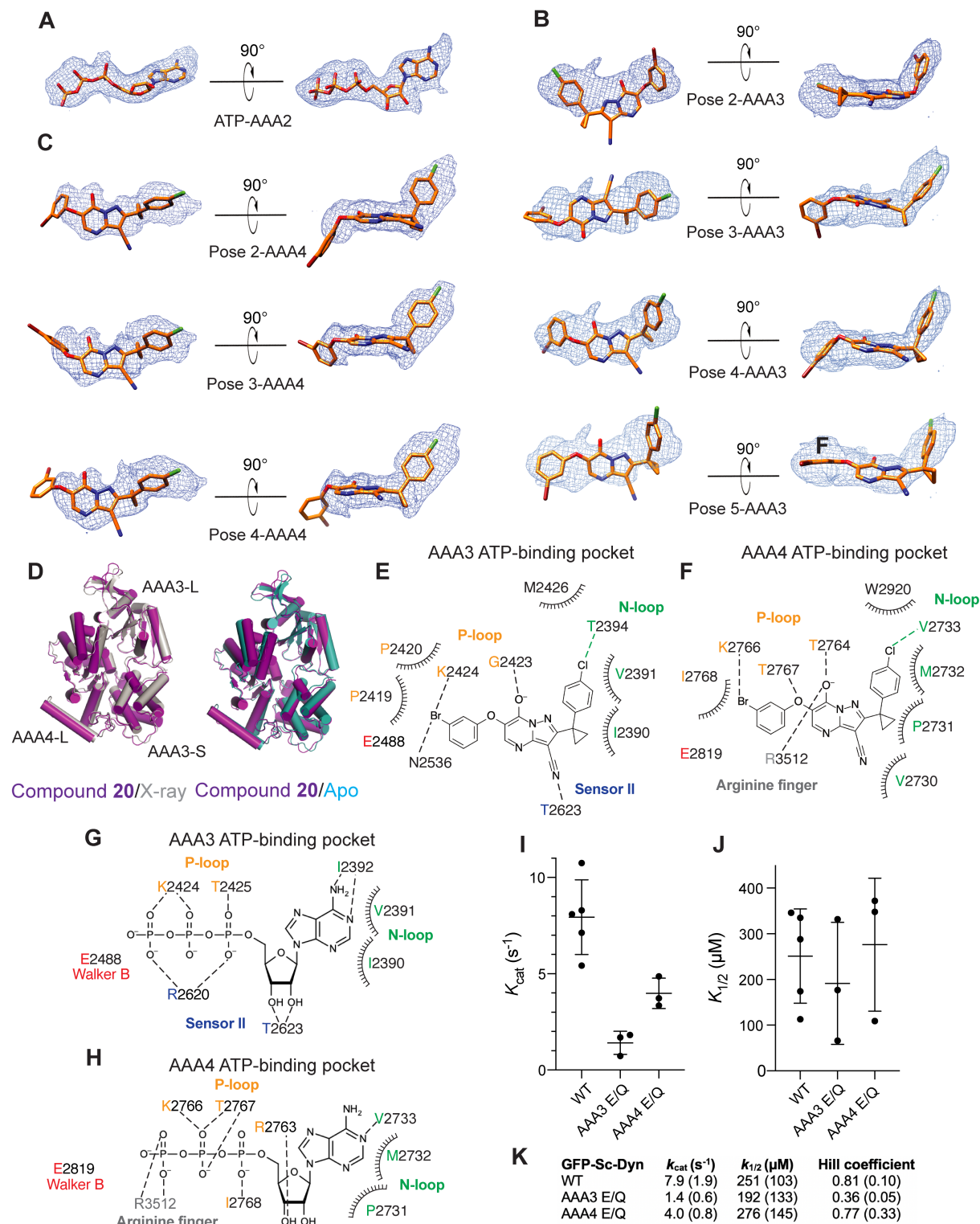


Figure S5. Analysis of compound binding to Sc-Dyn-lysoMut, Related to Figures 4 and 5. (A) Orientation of ATP in the AAA2 site generated by the GlideEM script and overlaid with the EM density (Map 4, blue mesh). ATP is shown as a stick model

(carbon: orange, oxygen: red, nitrogen: blue). (B, C) Poses of compound **20** generated by the Glide EM script for the AAA3 (B) and AAA4 (C) sites and overlaid with the EM density (Map 4, blue mesh). Compound **20** is shown as a stick model (carbon: orange, oxygen: red, nitrogen: blue, chlorine: green, bromine: dark red). (D) Comparison of the AAA3 domain between the cryo-EM reconstruction of Map 3 (magenta) and either the X-ray model (gray) or apo-model (cyan). Models are aligned on the AAA3-L subdomain. (E, F) Schematic for the predicted hydrogen bonding (black dashed lines), halogen bonding (green dashed lines) and van der Waals interactions (ticked curved lines) between compound **20** and the N-loop, P-loop, arginine finger, or sensor II motifs (N-loop: green, P-loop: yellow, arginine finger: gray, sensor II: blue, Walker B: red) in the AAA3 (E) or AAA4 (F) nucleotide-binding pockets. (G, H) Schematic for the hydrogen bonding (black dashed lines) and van der Waals interactions (ticked curved lines) between ATP and the N-loop, P-loop, arginine finger, sensor II or Walker B motifs (N-loop: green, P-loop: yellow, arginine finger: gray, sensor II: blue, Walker B: red) in the AAA3 (G) or AAA4 (H) nucleotide-binding pockets. Interactions are based on those observed in the AMPPNP-model (PDB: 4W8F). (I, J) Catalytic turnover number (k_{cat} ; I) and ATP concentration required for half-maximal velocity ($k_{1/2}$; J) of GFP-Sc-Dyn (n=5) and its mutants (n=3). Data represent average \pm SD Basal ATPase activity of the double mutant (AAA3/AAA4 E/Q) was too weak to accurately determine the construct's enzymatic parameters. (K) Values for enzymatic activity parameters of GFP-Sc-Dyn and its mutants are provided (mean, SD in parentheses).

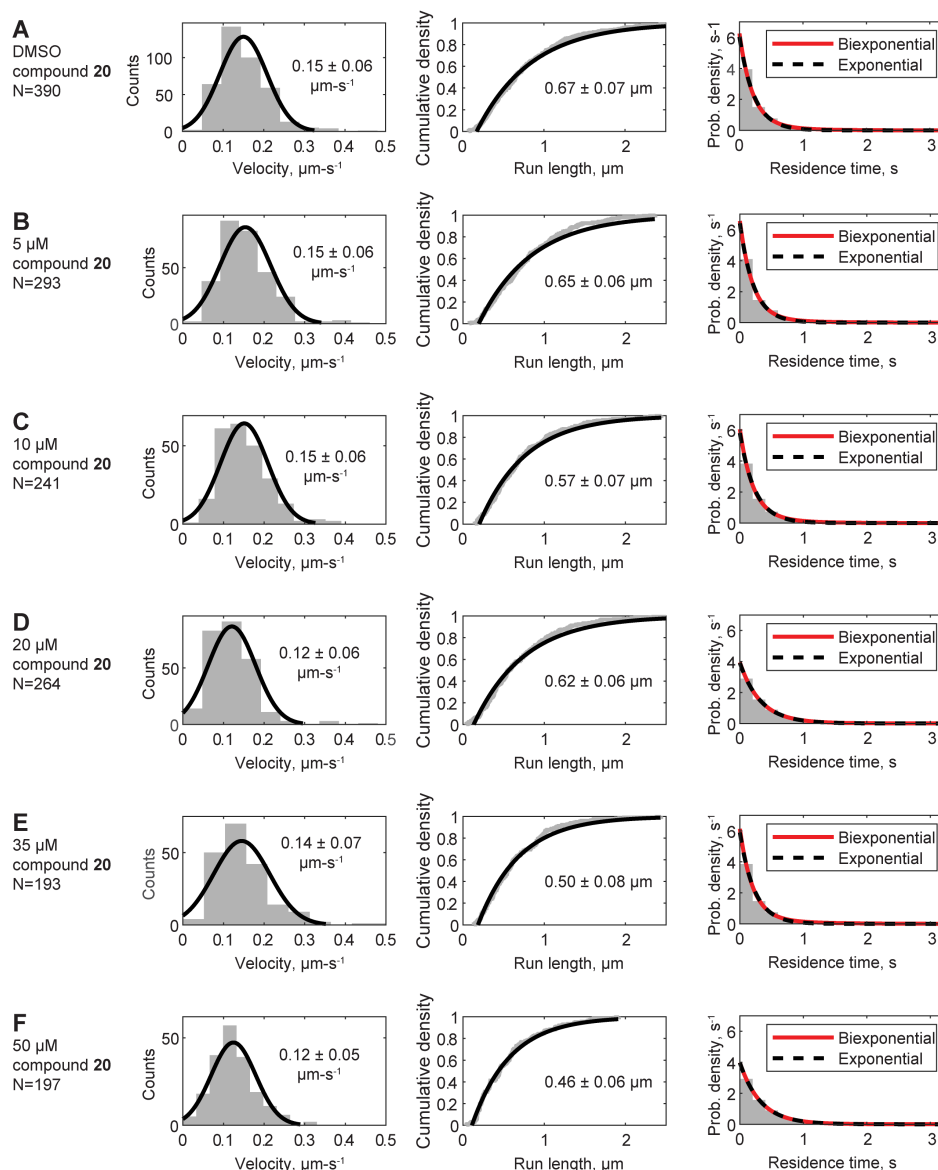


Figure S6. Effect of compound 20 on the velocity, run length, and pause density of Sc-DynGST, Related to Figure 7. (A-F) All data are pooled from $n=3-4$ independent experiments, with the number of events depicted in each panel. Velocities are shown with fit to a normal distribution, data reported as mean \pm SD. Run length distributions are shown as cumulative density function with offset exponential fit. Right most column of data shows the probability distribution of residence times of individual Sc-DynGST molecules within 50-nm bins along the direction of motion, following a published method (DeWitt et al., 2015). Fitting to single exponentials (black dashed lines) and bi-exponentials (red lines) yielded nearly identical results.

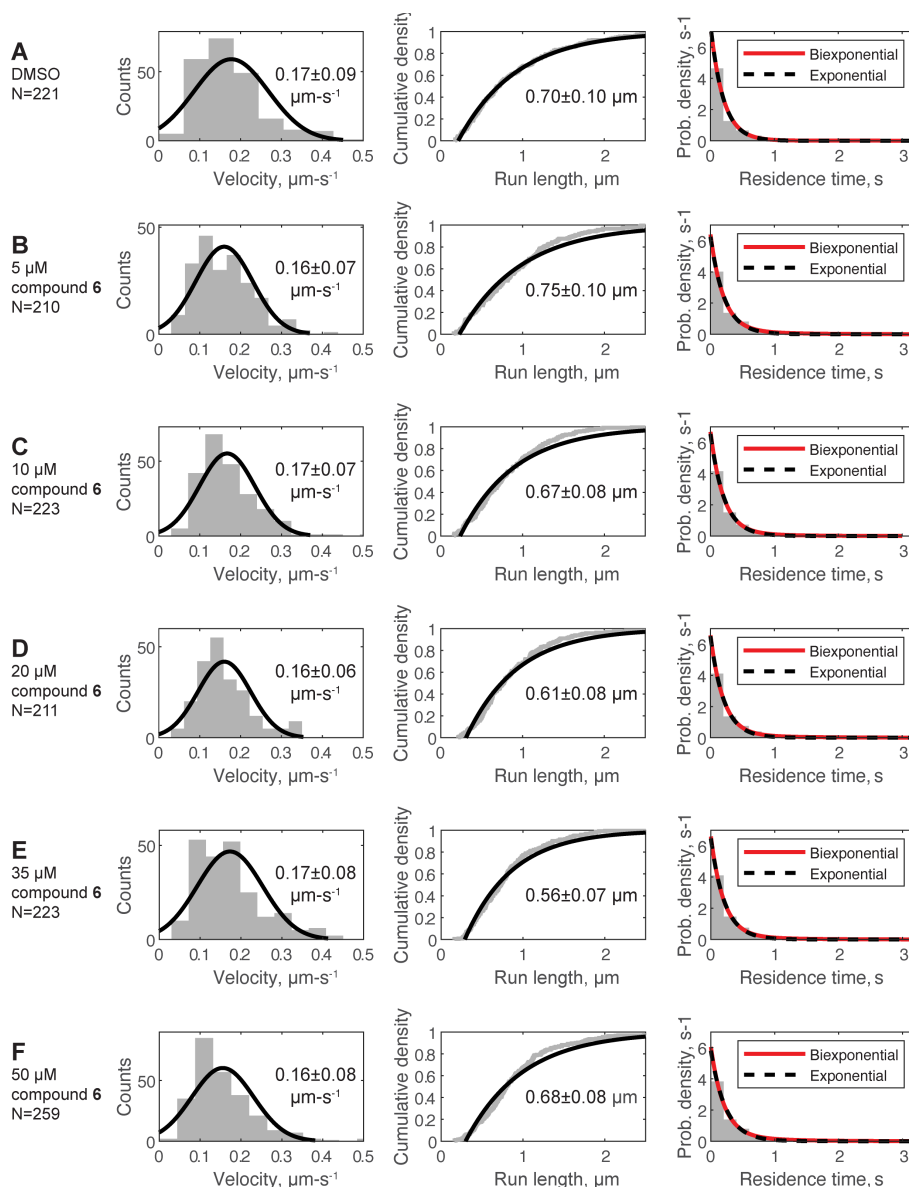


Figure S7. Effect of compound 6 on the velocity, run length, and pause density of Sc-DynGST, Related to Figure 7. (A-F) All data are pooled from $n=3$ independent experiments, with the number of events depicted in each panel. Velocities are shown with fit to a normal distribution, data reported as mean \pm SD. Run length distributions are shown as cumulative density function with offset exponential fit. Right most column of data shows the probability distribution of residence times of individual Sc-DynGST molecules within 50-nm bins along the direction of motion, following a published method (DeWitt et al., 2015). Fitting to single exponentials (black dashed lines) and bi-exponentials (red lines) yielded nearly identical results.